Journal of Power Sources 273 (2015) 624–630

Contents lists available at ScienceDirect

Journal of Power Sources

journal homepage: www.elsevier.com/locate/jpowsour

Pt nanoparticles supported on graphene three-dimensional network structure for effective methanol and ethanol oxidation

Mingjun Wang [a], Xuefen Song [a, b], Qi Yang [a], Hao Hua [a], Shuge Dai [a], Chenguo Hu [a, *], Dapeng Wei [b, **]

[a] Department of Applied Physics, Chongqing University, Chongqing 400044, PR China
[b] Key Laboratory of Multi-scale Manufacturing Technology, Chongqing Institute of Green and Intelligent Technology, Chinese Academy of Sciences, Chongqing 400714, PR China

HIGHLIGHTS

- Graphene three-dimensional network (G3DN) structure is prepared by CVD on a Si substrate.
- Pt/G3DN catalyst shows tremendous catalytic activity, excellent long term cycle stability.
- Wavy nanosheet channels are beneficial to diffusion of liquid reactants into catalyst sites.
- The channels result in reduction of liquid sealing effect greatly.

GRAPHICAL ABSTRACT

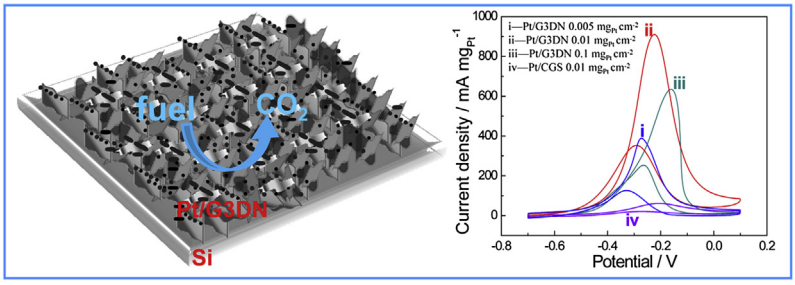

ARTICLE INFO

Article history:
Received 3 July 2014
Received in revised form
17 September 2014
Accepted 18 September 2014
Available online 30 September 2014

Keywords:
Graphene
Platinum catalyst
Electrooxidation
Methanol
Ethanol

ABSTRACT

We report a graphene three-dimensional network (G3DN) structure on a Si substrate, which is used as Pt nanoparticle support for effective electrocatalytic oxidation of methanol and ethanol. The controllable Pt loading on the G3DN is conducted by a facile, repeatable and environmentally friendly approach. The influence of graphene architecture on electrocatalytic activities is comparatively investigated by loading the same amount of Pt on the G3DN and on commercial graphene sheets (CGS). The Pt/G3DN (0.01 mg_{Pt} cm^{-2}) electrode exhibits a tremendous electrocatalytic activity for the oxidation of methanol and ethanol with oxidation current of 910.11 mA mg_{Pt}^{-1} and 246.69 mA mg_{Pt}^{-1} respectively owing to its high density of three-dimensional active sites, wavy sheet-network channels and synergistic effect of Pt and graphene. The peak current density ratio of the forward to backward potential scan is 2.79 and 0.65 for the methanol and ethanol oxidation respectively. The results reveal excellent characteristics of the Pt/G3DN electrode, such as easy preparation, high catalytic activity, stability and tolerance toward poisoning effects for the electrooxidation of methanol.

1. Introduction

Fuel cells have been generally recognized as a promising power source for daily transportation vehicles and portable electronic devices, because they convert the chemical energy of a fuel directly into electrical energy without a mechanical transmission and high pollutant discharge [1–4]. Direct alcohol fuel cells (DAFCs), one type of the direct fuel cells, use liquid alcohol as a fuel without a

* Corresponding author. Tel.: +86 2365620880; fax: +86 2365678362.
** Corresponding author.
E-mail addresses: wang_mj890@126.com (M. Wang), xfsong@cigit.ac.cn (X. Song), yangqi837@163.com (Q. Yang), bearhua1988@163.com (H. Hua), 1039880344@qq.com (S. Dai), hucg@cqu.edu.cn, hu_chenguo@yahoo.com (C. Hu), dpwei@cigit.ac.cn (D. Wei).

http://dx.doi.org/10.1016/j.jpowsour.2014.09.117
0378-7753/

reforming step, and have a simple-compact system with higher energy density than that of gaseous fuel cells. They can work at ambient temperature and observably avoid the difficulty of thermal management for small systems. Compared with rechargeable batteries, DAFCs can supply continuous power as long as methanol or ethanol is furnished. Methanol can be more efficiently oxidized than other alcohols, and ethanol is one of the most promising fuels with its low toxicity, abundance, low permeability across proton exchange membrane [5] and higher energy density (1325.31 kJ mol^{-1}) than that of methanol (702.32 kJ mol^{-1}) [6]. In this energy conversion process, distribution of catalysts like Pt nanoparticles on different architectures of supports greatly determines the energy density and conversion efficiency. Hence, exploitation of architectures with porous or 3D structure for catalyst loading is a challenging and significant work.

There are a number of support materials for Pt catalysts, such as SnO_2 flower-like crystals [7], TiO_2 spheres [8], carbon microspheres [9,10], carbon fibers [11], carbon nanotubes [12–14], graphene [15–20], etc. Carbon materials have been studied widely as electrocatalyst supports because of their good conduction, chemical stability and low cost. Among these carbon materials, graphene that consists of carbon atoms arranged in a honeycomb lattice has received tremendous attention since it was experimentally discovered in 2004 [21]. And graphene has notable advantages such as electrical conductivity, large specific surface area, chemical stability and easy adsorption of catalyst nanoparticles, which can be used to construct a highly efficient catalyst electrode for fuel cells. However, there are some problems with the catalyst electrode that is made by Pt nanoparticles supported on the graphene powder, such as the difficult preparation process, a little porous structure owing to the strong planar stacking of graphene sheets, and easy detachment of the graphene sheets from the substrate. Recently, graphene on three-dimensional Ni foam with pore size of 590 μm [22] has been used to support PtRu catalyst, which demonstrates enhanced catalytic activity for both methanol and ethanol oxidation, but the catalytic effect is not very satisfactory due to its too big pore size to form high density catalytic sites. Although the 3D framework of graphene oxide with a loading of Pt/PdCu nanoparticles deposited on a glassy carbon electrode presents a high efficiency of ethanol oxidation [23], the complicated fabrication process and possible detachment of catalyst layer from the substrate are fatal disadvantages for its applications.

Herein, we report a graphene 3D network (G3DN) structure growing firmly and directly on a Si substrate by CVD method, which is used as Pt nanoparticle support for effective electrocatalytic oxidation of methanol and ethanol. The controllable Pt loading on the G3DN is conducted by a facile, repeatable and environmentally friendly approach. The G3DN and Pt/G3DN catalysts are characterized by Raman spectra, field emission scanning electron microscope (FESEM), energy-dispersive X-ray spectroscope (EDS) and high resolution transmission electron microscope (HRTEM). The performance of the Pt/G3DN catalyst for methanol and ethanol electrooxidation is studied via cyclic voltammetry (CV), linear sweep voltammetry (LSV) and chronoamperometry in alkaline medium. To find out the influence of graphene architecture, electrocatalytic activities are comparatively investigated by loading the same amount of Pt on the G3DN and commercial graphene sheets (CGS).

2. Experimental

2.1. Chemicals

$H_2PtCl_6 \cdot 6H_2O$, methanol, ethanol, Na_2SO_4, KOH and H_2SO_4 were purchased from Chongqing Chemical Reagent Company. Single side polished p-type silicon wafer (0.01–0.02 Ω cm, 500 ± 10 μm in thickness, crystal orientation <100>) was purchased from Zhejiang Lijing Optoelectronic Technology Co., Ltd. Commercial graphene (SGNP-F01005) was purchased from Nanjing SCF Nanotech, Ltd. Nafion® and silver paste were purchased from Sigma–Aldrich and SPI Supplies. All chemicals were of analytical grade and were used as received. Deionized water was used throughout.

2.2. Preparation of Pt/G3DN and Pt/CGS catalyst electrodes

The G3DN was prepared by CVD method. In a typical experiment, a Si wafer was washed in acetone and ethanol by turns for 30 min, then rinsed with deionized water and dried for use. Next, the Si wafer was placed into the center of a quartz tube, which was then heated to 750 °C under a constant flow of H_2 gas. And the Si wafer was first exposed to hydrogen plasma for 10 min. Then, CH_4 was flown into the chamber, and was mixed with H_2 gas (typically specific flow ratio of CH_4 and H_2 is 3/2) under a pressure of 50 Pa and then the condition was maintained for 2 h. Finally, the G3DN sample was obtained after it cooled down to room temperature.

The as-prepared G3DN/silicon wafer was cut into squares of 10 mm × 10 mm, and then 10 μL of 2.564 mM, 2 × 2.564 mM and 20 × 2.564 mM chloroplatinic acid ethanol solution were dropped onto the squares respectively, and then they were allowed evaporate slowly at room temperature until they were completely dry. Then these 3 G3DN/silicon squares were calcined at 400 °C in a vacuum tube furnace for 10 min to thermally decompose $H_2PtCl_6 \cdot 6H_2O$. Finally, the Pt/G3DN catalysts with Pt surface density of 0.005 mg cm^{-2} (i), 0.01 mg cm^{-2} (ii) and 0.1 mg cm^{-2} (iii) were obtained after washing with deionized water and drying in air. The Pt/G3DN catalyst electrode was obtained by connecting the catalyst square with a copper wire using silver paste and then covering it with epoxy resin, but with 5 mm × 8 mm area left open. To compare the catalysis of the Pt catalyst supported on G3DN/Si with common Pt supported on graphene powder, Pt supported on CGS/Si was prepared with a loading of 0.01 mg cm^{-2} Pt. The fabrication of the Pt supported on CGS/Si was carried out according to the following steps: a certain amount of CGS dispersed in ethanol solution was dropped onto a 10 mm × 10 mm silicon sheet, the surface of which was purposely made rough for the graphene powder to adhere. 10 μL of 2 × 2.564 mM chloroplatinic acid ethanol solution was dropped onto CGS/Si; then the $H_2PtCl_6 \cdot 6H_2O$/CGS/Si was calcined to get the Pt/CGS/Si. To immobilize the Pt/CGS nanostructures on the silicon substrate and to improve the anti-interference ability, 5 μL of 0.5 wt% Nafion was dropped onto the surface of the electrode. Finally, the Pt/CGS electrode was obtained with a Pt surface density of 0.01 mg cm^{-2} (iv) and had same working area following the same process as the Pt/G3DN/Si electrode fabrication.

2.3. Characterization of Pt/G3DN and Pt/CGS catalysts

Raman spectra were taken to characterize the G3DN and CGS by using Witec confocal Raman microscopy (Lab RAM HR Evolution). The morphology of the G3DN, Pt/G3DN and Pt/CGS were characterized by FESEM (Nova 400 Nano SEM) and TEM (JEOL4000EX). The thickness of the Pt/G3DN and Pt/CGS films were measured by FESEM and the chemical compositions were analyzed by energy-dispersive X-ray spectroscopy (EDS, Oxford).

2.4. Electrochemical measurement

Electrochemical measurement was carried out with a conventional three-electrode electrochemical cell by using electrochemical workstation (CHI 660D). A platinum foil electrode

(15 mm × 10 mm × 0.3 mm in length, width and thickness) and Ag/AgCl (saturated KCl) were used as the counter and reference electrodes respectively. CV and LSV were conducted at a rate of 50 mV s^{-1} and 5 mV s^{-1} respectively in alkaline or acidic aqueous solution. The chronoamperometry was recorded in alkaline aqueous solution at −0.25 V or in acidic aqueous solution at 0.7 V for 2000 s. The electrochemical impedance spectroscopy (EIS) was measured in 0.1 M Na_2SO_4 aqueous solution at frequency ranging from 0.5 Hz to 1000,000 Hz with amplitude at 5 mV. All the experiments were carried out at room temperature (20 °C).

3. Results and discussion

3.1. Characterization

Raman spectra of the G3DN and CGS are shown in Fig. 1. The ratios of 2D peak to G peak of the two samples indicate few-layer graphene. In addition, a relatively high intensity of D peak of G3DN is observed, which indicates the presence of a significant number of defects at the surface edges or bend points, which might be good anchoring sites for Pt nanoparticles.

The details of the Pt/G3DN (ii) are characterized by TEM and HRTEM in Fig. 2a and b, respectively, which suggest a lot of Pt single crystal particles with sizes ranging from 3 to 20 nm on the surface of wavy graphene network. Fig. 2c shows TEM image of the Pt/G3DN (i), indicating more uniform Pt particles with sizes ranging from 3 to 10 nm on the surface of the graphene network. Fig. 2d shows FESEM image of the Pt/G3DN (iii), indicating uniform Pt nanocrystal particles with sizes ranging from 10 to 20 nm. The typical low magnification FESEM image in Fig. 3a shows the uniform growth of the pure G3DN, and the high magnification FESEM image in Fig. 3b shows that pure G3DN is formed by a large number of crisscrossed wavy graphene nanosheets due to the existence of a large number of defects, which agrees with the Raman spectrum in Fig. 1. The surface morphology of the G3DN almost remains unchanged after being coated with Pt NPs, as shown in Fig. 3c. FESEM image in Fig. 3d shows a flat morphology of CGS on Si substrate without three-dimensional structure. The thickness of the Pt/G3DN (ii) and the Pt/CGS are 1 μm and 60 μm, respectively (the insets in Fig. 3c and d). The Pt/CGS is much thicker than that of the Pt/G3DN (ii). This thickness has to be reached if Si substrate is fully covered by the commercial graphene powder due to aggregation effect of powder. Both EDS results demonstrate that the contained elements are platinum and carbon (silicon and fluorine are from the substrate and Nafion respectively).

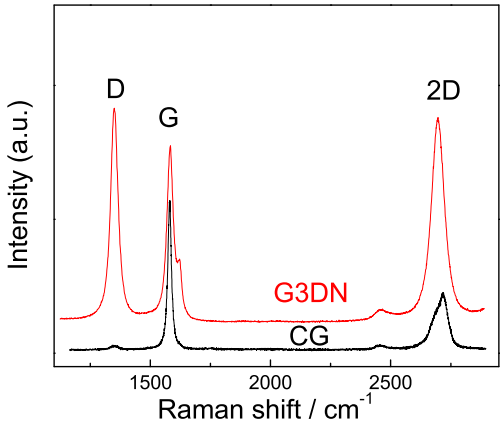

Fig. 1. Raman spectra of the G3DN and CGS.

3.2. Electrooxidation of methanol and ethanol

The CVs taken in 1.0 M KOH for the Pt/G3DN/Si and Pt/CGS/Si electrodes (with same geometric area) are shown in Fig. 4. There are two peaks at −0.741 V and −0.656 V due to hydrogen adsorption/desorption for the three Pt/G3DN/Si electrodes. Obviously, the peaks of the electrode (iii) are much stronger than that of the electrode (ii) and electrode (i) because of more Pt loading. The desorption peaks of the electrode (ii) are stronger than that of the electrode (iv), which suggests that the Pt/G3DN/Si catalyst has better catalytic activity than that of the Pt/CGS/Si catalyst. The electrochemical active surface (EAS) is calculated according to the area of hydrogen adsorption/desorption peaks [24]. The EAS is 15.39 m^2 g^{-1}, 15.64 m^2 g^{-1} and 10.57 m^2 g^{-1} and 14.71 m^2 g^{-1} for the electrode (i), (ii), (iii) and (iv) in alkaline media respectively, indicating a more effective catalysis of the electrode (ii) than that of the electrode (iv), and a decrease in the EAS with an increase in platinum loading. The more effective catalysis is attributed to three-dimensional network structure with channels and pores on the surface of the electrode, by which liquid sealing effect can be greatly reduced and liquid fuel can easily diffuse to the catalyst sites and the exhaust of gaseous product (CO_2 or CO) can effectively escape from the catalyst sites.

Fig. 5a and b shows the CVs of the ethanol (Fig. 5a) and methanol (Fig. 5b) electrooxidation on the electrode (i), (ii), (iii) and (iv) in 1.0 M KOH aqueous solution. For a better comparison, some data from the CVs are also listed in Table 1, from which we find that the peak potential gets lower with the decrease in platinum loading for the electrode (i), (ii) and (iii). Though the three Pt/G3DN/Si electrodes have the same geometric working area, the electrode (ii, 0.01 mg_{Pt} cm^{-2}) has much higher peak current density J_P (versus unit mass of Pt) due to its larger active surface than other electrodes. Obviously, the peak current density J_P' (versus unit area of electrode) of the Pt/G3DN/Si can be quickly improved by increasing the platinum loading. That the J_P of the electrode (i) is less than that of the electrode (ii) may be a result of easier hydrocarbon adsorption on the electrode (i), and that the J_P of the electrode (iii) is less than that of the electrode (ii) may be a result of bigger size of Pt particles (due to the particle congregation) on the electrode (iii), which is consistent with the comparison of EAS (versus unit mass of Pt). Besides, the ratio of the peak current density (I_f) in forward scan to the peak current density (I_b) in backward scan, I_f/I_b, can be used to describe an electrode tolerance to the accumulation of carbonaceous species [25]. A higher ratio indicates a better oxidation of alcohol into CO_2 in forward scan and relatively less carbonaceous residues on the surface of the electrode. In Table 1, the ratio is 3.08, 2.79 and 2.51 for the electrode (i), (ii) and (iii) for the methanol oxidation, respectively, indicating that the Pt loading on the three-dimensional network structure presents a good tolerance. The ratio is 1.04, 0.65 and 0.61 for the electrode (i), (ii) and (iii) in the ethanol oxidation respectively, indicating that smaller size of Pt particles on the three-dimensional network structure present better tolerance to the accumulation of carbonaceous species. Although the high I_f/I_b ratios are obtained for both methanol and ethanol electrooxidation on the electrode (iv), the peak current densities are very small because of its planar stacking of graphene sheets.

To further study the catalysis, LSVs are conducted at very slow potential scan rate of 5 mV s^{-1}, as shown in Fig. 5c and d for ethanol and methanol respectively. The peak current densities on the four electrodes are in the order of electrode (ii) > (iii) > (i) > (iv) for methanol electrooxidation and electrode (ii) > (i) > (iii) > (iv) for ethanol electrooxidation. Obviously, the electrode (ii) exhibits extremely highest oxidation current density among these quasi-steady-state polarization curves. This suggests that the three-dimensional network structure, size of Pt nanoparticles and a

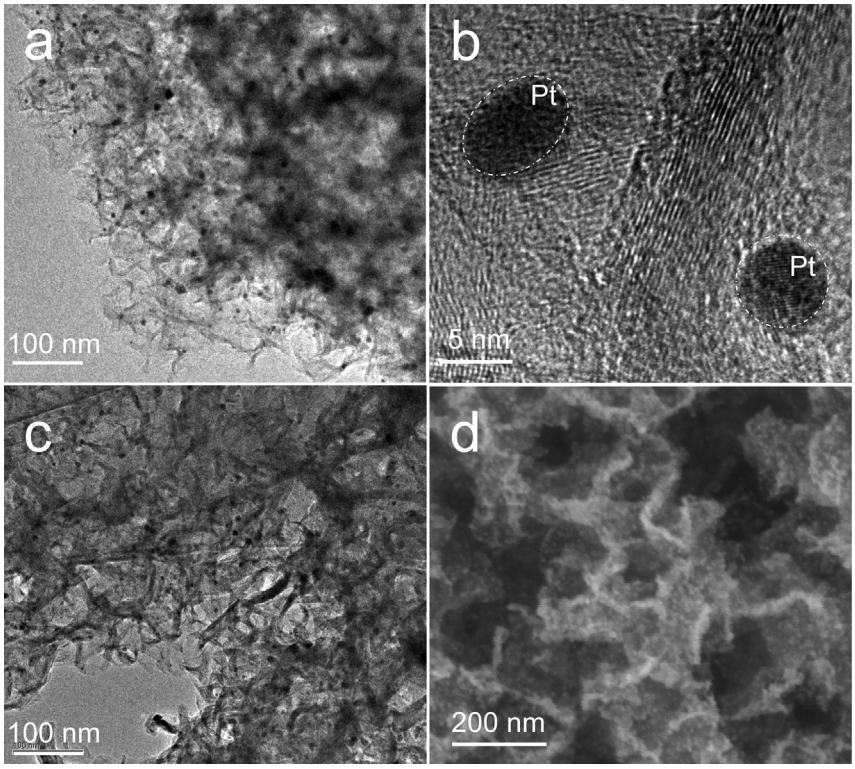

Fig. 2. TEM (a) and HRTEM (b) images of the Pt/G3DN (ii). TEM image (c) of the Pt/G3DN (i). FESEM image (d) of the Pt/G3DN (iii).

proper amount of Pt loading can greatly enhance the electrocatalytic activity towards methanol and ethanol oxidation. The results observed here are in agreement with the CV studies, except that for the electrode (iv) there might exist a severe liquid sealing effect due to its none three-dimensional network structure.

The catalytic activity and stability of the electrode (i), (ii), (ii) and (iv) for methanol and ethanol electrooxidation have been investigated by chronoamperometries in Fig. 5e and f, respectively, and steady decrease in current are seen within the first few minutes for the four electrocatalysts, followed by a fairly constant current for

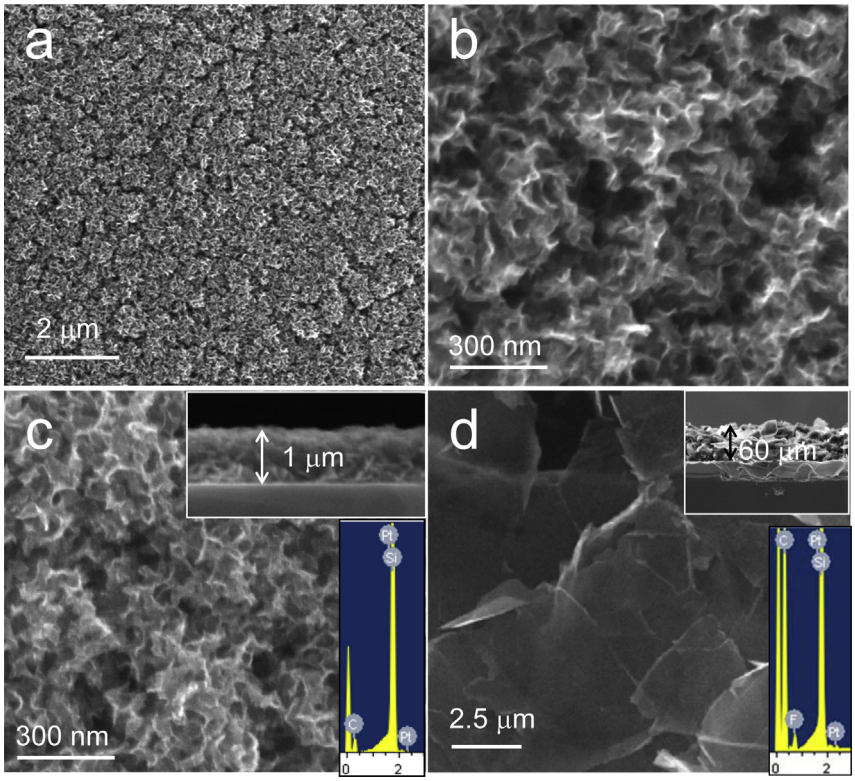

Fig. 3. FESEM images of the pure G3DN (a, b), Pt/G3DN (ii) (c) and Pt/CGS (iv) (d). The insets are the corresponding thickness and EDS.

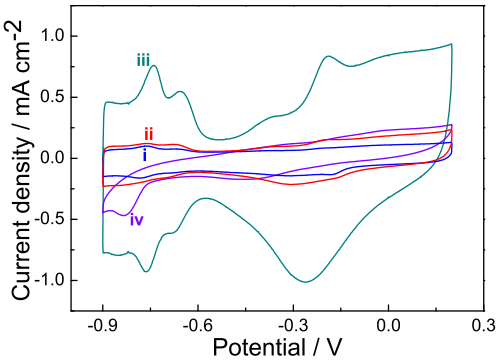

Fig. 4. CVs of the Pt/G3DN electrode (i), (ii), (iii) and Pt/CGS electrode (iv) in 1.0 M KOH aqueous solution at sweep rate of 50 mV s^{-1}.

longer time. Fig. 5e and f reveals that the ultimate steady current density for methanol electrooxidation on the electrode (ii) is 125.05 mA mg_{Pt}^{-1}, which is higher than that on the electrode (i) (55.42 mA mg_{Pt}^{-1}), electrode (iii) (27.76 mA mg_{Pt}^{-1}) and electrode (iv) (2.67 mA mg_{Pt}^{-1}). Furthermore, higher initial current means more active sites available for the oxidation. It is demonstrated that higher catalytic activity and better stability are achieved on the electrode (ii) for the methanol electrooxidation.

Besides, we choose electrode (ii) to measure its catalysis in acidic media, as shown in Fig. 6. Though it has similar EAS as that in alkaline medium, it only shows the peak current density of 93.57 mA mg_{Pt}^{-1} and 141.22 mA mg_{Pt}^{-1}, and long term cycle stability current density of 4.00 mA mg_{Pt}^{-1} and 15.80 mA mg_{Pt}^{-1} at the 2000th second for the oxidation of methanol and ethanol respectively. The results reveal a poorer performance in acidic media than that in alkaline media, which might be attributed to the difficulty in scavenging CO_2 in acidic media.

The excellent catalysis to electrooxidation of methanol and ethanol on the electrode (ii) is caused from the 3D network-structure catalytic sites and the good distribution of the Pt nanoparticles on this structure, as shown in Fig. 7. On the other hand, the wavy channels in the electrode (ii) also improve the diffusion of liquid reactants into the catalyst sites and result in reduction of liquid sealing effect greatly. The reduction of liquid sealing effect in turn increases the active surface area for electrochemical reactions [26]. Furthermore, the CO tolerance of Pt can be improved by relaxing the strong CO adsorption on Pt due to the interaction between Pt and graphene [22].

It is well known that the electrochemical impedance spectroscopy (EIS) technique is a powerful tool for characterizing the electrochemical processes occurring at the solution/electrode interface. Fig. 8 presents Nyquist plots for the electrode (i), (ii), (iii) and (iv) in 0.1 M Na_2SO_4 at frequency ranging from 0.5 Hz to

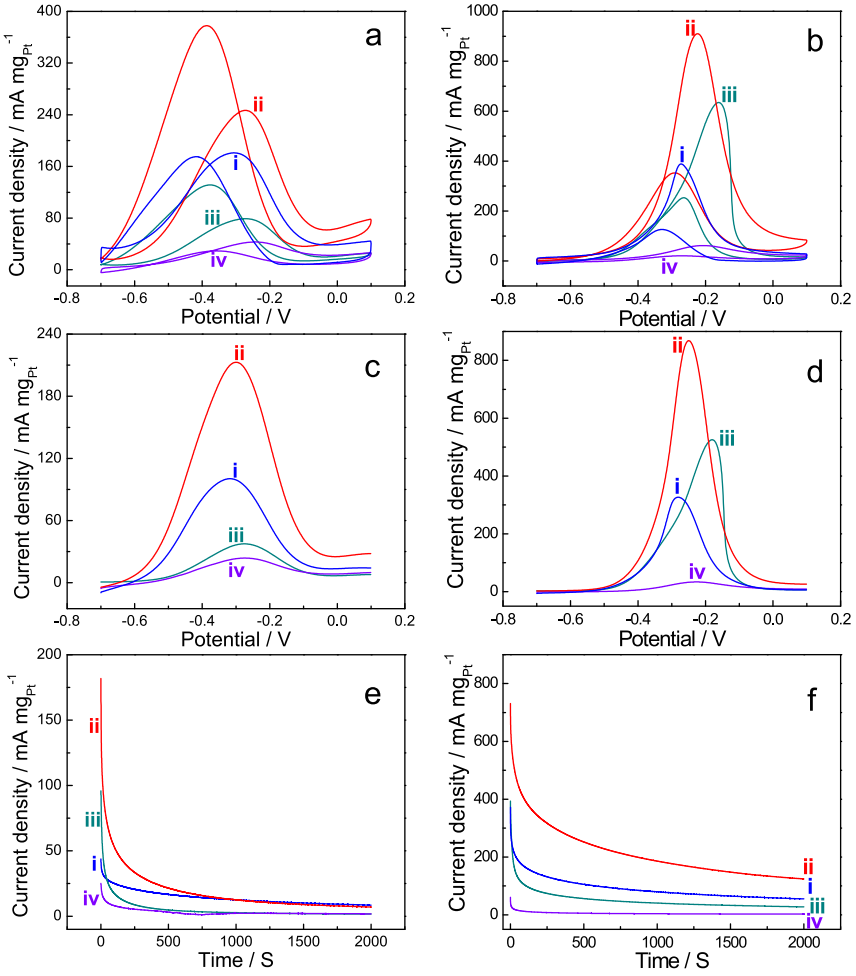

Fig. 5. CVs of the Pt/G3DN electrode (i), (ii), (iii) and Pt/CGS electrode (iv) in 1.0 M KOH aqueous solution containing 1.0 M ethanol (a) or 1.0 M methanol (b) at sweep rate of 50 mV s^{-1}. The corresponding LSVs for the ethanol (c) or methanol (d) oxidation measured at sweep rate of 5 mV s^{-1}. The corresponding chronoamperometry diagrams measured at −0.3 V for the ethanol oxidation (e) or −0.25 V for the methanol oxidation (f) for 2000 s.

Table 1
Comparison of the performance of the three Pt/G3DN/Si electrodes and Pt/CGS/Si electrode.

Electrodes	Peak potential (V)		J_P (mA mg_{Pt}^{-1})		J_P' (mA cm^{-2})		I_f/I_b ratio	
	Methanol	Ethanol	Methanol	Ethanol	Methanol	Ethanol	Methanol	Ethanol
i (alkaline)	−0.27	−0.31	388.63	181.26	1.94	0.91	3.08	1.04
ii (alkaline)	−0.22	−0.27	910.11	246.69	9.10	2.47	2.79	0.65
iii (alkaline)	−0.16	−0.27	634.71	79.06	63.47	7.91	2.51	0.61
iv (alkaline)	−0.21	−0.24	61.79	43.01	0.62	0.43	2.98	1.47
ii (acidic)	0.65	0.70	93.31	141.42	0.93	1.41	1.28	0.88

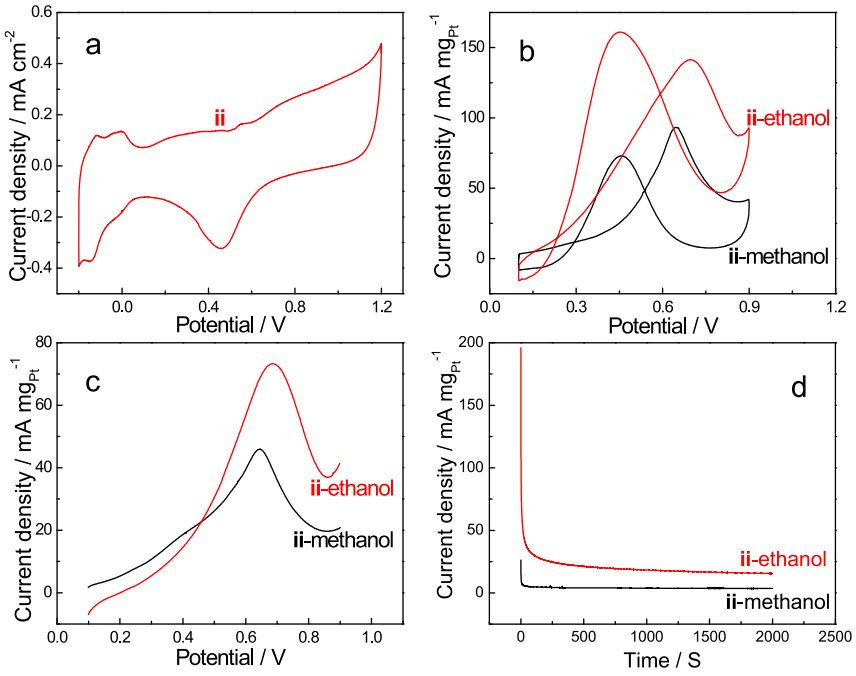

Fig. 6. CVs of the Pt/G3DN electrode (ii) in 0.5 M H_2SO_4 aqueous solution (a), 0.5 M H_2SO_4 aqueous solution containing 1.0 M ethanol or 1.0 M methanol (b) at sweep rate of 50 mV s^{-1}. The corresponding LSVs measured at sweep rate of 5 mV s^{-1} (c). The corresponding chronoamperometry diagrams measured at 0.7 V for 2000 s (d).

1000 kHz. The Nyquist plot includes a semicircle region lying on the Z'-axis at higher frequency (it is related to the electron-transfer-limited process), and a linear part at lower frequency (it is related to the diffusion limited process). Usually, the semicircle diameter equals to the electron-transfer resistance, which is obviously affected by the surface modification of the electrode [27]. As shown in Fig. 8, the electron-transfer resistance of the three Pt/G3DN electrodes are much less than that of the Pt/CGS electrode,

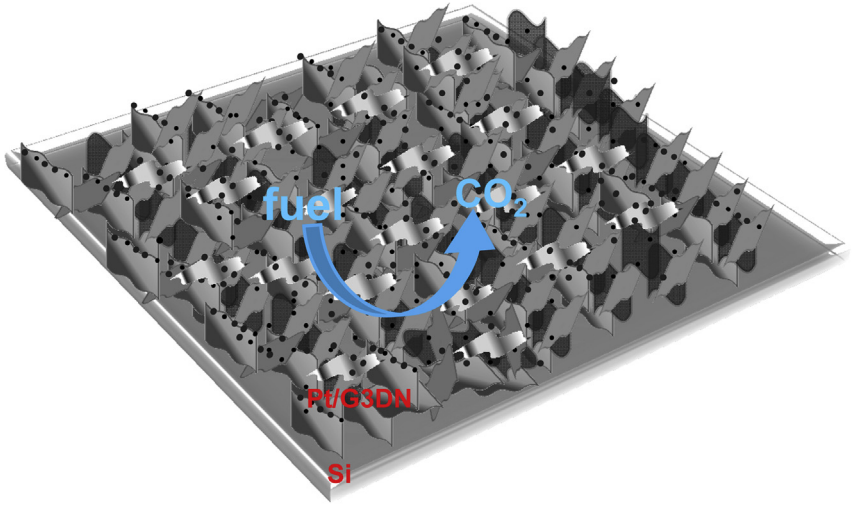

Fig. 7. Schematic diagram of the Pt/G3DN catalyst with 3D platinum distribution that improves the diffusion of liquid reactants into the catalyst sites and reduces liquid sealing effect.

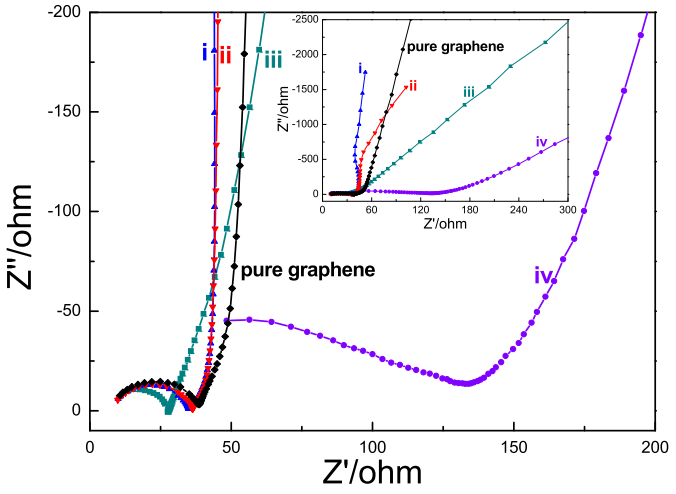

Fig. 8. Magnified Nyquist plot at high frequency of the G3DN, Pt/G3DN electrode (i), (ii), (iii) and Pt/CGS electrode (iv), and Nyquist plot (inset).

indicating that the three-dimensional network structure can enhance the conductivity of the electrode owing to its better contact with Si substrate, and to its less thickness for faster interfacial charge carrier transfer in comparison with the CGS. Besides, the electron-transfer resistance of the three Pt/G3DN electrodes is very close to that of the pure G3DN electrode, and the electron-transfer resistance decrease with an increase in platinum loading. Conductivity and surface activity are two important factors for a good analytical electrode [28,29]. As the wavy nanosheet structure not only provides the network channels for a better diffusion of liquid reactants into the catalyst sites, but also retains faster electron-transfer speed on the interface between liquid and electrode, the Pt/G3DN electrode (ii) possesses excellent performance in electrooxidation of methanol.

4. Conclusions

A repeatable, simple, convenient, feasible and environmentally friendly approach has been employed to fabricate a Pt/G3DN catalyst electrode with controllable platinum loading for alcohol fuel cells. The three-dimensional nanosheet network structure of Pt/G3DN catalyst electrode exhibits a highly catalytic oxidation activity for methanol and ethanol in alkaline solution. The series of electrochemical measurement demonstrate that both the wavy network channels for a better diffusion of liquid fuel into the catalyst sites and the faster electron transfer on the interface between liquid and electrode are very important for the promotion of methanol and ethanol electrooxidation. Our investigations suggest that the Pt/G3DN (0.01 $mg_{Pt}\,cm^{-2}$) electrocatalyst could be adopted as excellent catalyst in DAFCs, owing to its superior electrocatalytic current density of 910.11 mA mg_{Pt}^{-1} and 246.69 mA mg_{Pt}^{-1}, long term cycle stability, and large I_f/I_b ratio for the oxidation of methanol and ethanol respectively, while the Pt/CGS exhibits poorer catalytic performance. In addition, the peak current density (versus unit area of electrode) of the Pt/G3DN/Si electrode can be greatly improved by increasing the platinum loading.

Acknowledgments

This work is supported by the NSFCQ (cstc2012jjB0006), SRFDP (20110191110034, 20120191120039), NSFC (11204388, 11374359), and the Project-sponsored by SRF for ROCS, SEM.

References

[1] J.P. Pereira, D.S. Falcão, V.B. Oliveira, A.M.F.R. Pinto, J. Power Sources 256 (2014) 14–19.
[2] X.Y. Yong, J. Feng, Y.L. Chen, D.Y. Shi, Y.S. Xu, J. Zhou, S.Y. Wang, L. Xu, Y.C. Yong, Y.M. Sun, C.L. Shi, P.K. OuYang, T. Zheng, Biosens. Bioelectron. 56 (2014) 19–25.
[3] Z.Y. Shih, C.W. Wang, G.B. Xu, H.T. Chang, J. Mater. Chem. A 1 (2013) 4773–4778.
[4] B.E. Logan, B. Hamelers, R. Rozendal, U. Schröder, J. Keller, S. Freguia, P. Aelterman, W. Verstraete, Korneel Rabaey, Environ. Sci. Technol. 40 (2006) 5181–5192.
[5] S.Q. Song, P. Tsiakaras, Appl. Catal. B 63 (2006) 187–193.
[6] J.M. Léger, J. Appl. Electrochem. 31 (2001) 767–771.
[7] H.L. Zhang, C.G. Hu, X.S. He, H. Liu, G.J. Du, Y. Zhang, J. Power Sources 196 (2011) 4499–4505.
[8] H. Hua, C.G. Hu, Z.H. Zhao, H. Liu, X. Xie, Y. Xi, Electrochim. Acta 105 (2013) 130–136.
[9] C.W. Xu, L.Q. Cheng, P.K. Shen, Y.L. Liu, Electrochem. Commun. 9 (2007) 997–1001.
[10] C.W. Zhang, L.B. Xu, N.N. Shan, T.T. Sun, J.F. Chen, Y.S. Yan, ACS Catal. 4 (2014) 1926–1930.
[11] S.L. Chen, H.Q. Hou, F. Harnisch, S.A. Patil, A.A. Carmona-Martinez, S. Agarwal, Y.Y. Zhang, S. Sinha-Ray, A.L. Yarin, A. Greiner, U. Schröder, Energy Environ. Sci. 4 (2011) 1417–1421.
[12] J. Prabhuram, T.S. Zhao, Z.K. Tang, R. Chen, Z.X. Liang, J. Phys. Chem. B 110 (2006) 5245–5252.
[13] L. Cao, F. Scheiba, C. Roth, F. Schweiger, C. Cremers, U. Stimming, H. Fuess, L.Q. Chen, W.T. Zhu, X.P. Qiu, Angew. Chem. Int. Ed. 45 (2006) 5315–5319.
[14] Y. Cheng, C.W. Xu, P.K. Shen, S.P. Jiang, Appl. Catal. B 158 (2014) 140–149.
[15] N.G. Shang, P. Papakonstantinou, P. Wang, S. Ravi, P. Silva, J. Phys. Chem. C 114 (2010) 15837–15841.
[16] Y.J. Li, W. Gao, L.J. Ci, C.M. Wang, P.M. Ajayan, Carbon 48 (2010) 1124–1130.
[17] R. Ojani, J.B. Raoof, M. Goli, R. Valiollahi, J. Power Sources 264 (2014) 76–82.
[18] Y.T. Zhang, G. Chang, H.H. Shu, M. Oyama, X. Liu, Y.B. He, J. Power Sources 262 (2014) 279–285.
[19] J.N. Zheng, S.S. Li, F.Y. Chen, N. Bao, A.J. Wang, J.R. Chen, J.J. Feng, J. Power Sources 266 (2014) 259–267.
[20] S.J. Guo, S.J. Dong, E.K. Wang, ACS Nano 4 (2010) 547–555.
[21] K.S. Novoselov, A.K. Geim, S.V. Morozov, D. Jiang, Y. Zhang, S.V. Dubonos, I.V. Grigorieva, A.A. Firsov, Science 306 (2004) 666–669.
[22] C.C. Kung, P.Y. Lin, Y.H. Xue, R. Akolkar, L.M. Dai, X. Yu, C.C. Liu, J. Power Sources 256 (2014) 329–335.
[23] C.G. Hu, H.H. Cheng, Y. Zhao, Y. Hu, Y. Liu, L.M. Dai, L.T. Qu, Adv. Mater. 24 (2012) 5493–5498.
[24] A. Pozio, M. De Francesco, A. Cemmi, F. Cardellini, L. Giorgi, J. Power Sources 105 (2002) 13–19.
[25] S.B. Han, Y.J. Song, J.M. Lee, J.Y. Kim, K.W. Park, Electrochem. Commun. 10 (2008) 1044–1047.
[26] F.Y. Xie, Z.Q. Tian, H. Meng, P.K. Shen, J. Power Sources 141 (2005) 211–215.
[27] X.X. Zhong, J.H. Chen, B. Liu, Y. Xu, Y.F. Kuang, J. Solid State Electrochem. 11 (2007) 463–468.
[28] C.G. Hu, W.L. Wang, K.J. Liao, G.B. Liu, Y.T. Wang, J. Phys. Chem. Solids 65 (2004) 1731–1736.
[29] C.G. Hu, Y.Y. Zhang, G. Bao, Y.L. Zhang, M.L. Liu, Z.L. Wang, Chem. Phys. Lett. 418 (2006) 524–529.